Intrinsic Gating of Inward Rectifier in Bovine Pulmonary Artery Endothelial Cells in the Presence or Absence of Internal Mg^{2+}

MICHAEL R. SILVER and THOMAS E. DECOURSEY

From the Departments of Medicine and Physiology, Rush Medical Center, Chicago, Illinois 60612

ABSTRACT   Inward rectifier (IR) currents were studied in bovine pulmonary artery endothelial cells in the whole-cell configuration of the patch-clamp technique with extracellular K^+ concentrations, $[K^+]_o$, ranging from 4.5 to 160 mM. Whether the concentration of free Mg^{2+} in the intracellular solution, $[Mg^{2+}]_i$, was 1.9 mM or nominally 0, the IR exhibited voltage- and time-dependent gating. The IR conductance was activated by hyperpolarization and deactivated by depolarization. Small steady-state outward IR currents were present up to ~40 mV more positive than the K^+ reversal potential, E_K, regardless of $[Mg^{2+}]_i$. Modeled as a first-order $C \rightleftarrows O$ gating process, both the opening rate, α, and the closing rate, β, were exponentially dependent on voltage, with β more steeply voltage dependent, changing e-fold for 9 mV compared with 18 mV for an e-fold change in α. Over all $[K^+]_o$ studied, the voltage dependence of α and β shifted along with E_K, as is characteristic of IR channels in other cells. The steady-state voltage dependence of the gating process was well described by a Boltzmann function. The half-activation potential was on average ~7 mV negative to the observed reversal potential in all $[K^+]_o$ regardless of $[Mg^{2+}]_i$. The activation curve was somewhat steeper when Mg-free pipette solutions were used (slope factor, 4.3 mV) than when pipettes contained 1.9 mM Mg^{2+} (5.2 mV). The simplest interpretation of these data is that IR channels in bovine pulmonary artery endothelial cells have an intrinsic gating mechanism that is not due to Mg block.

INTRODUCTION

Endothelial cells, which constitute a confluent monolayer lining all blood vessels, recently have been found to play a role in modulation of vascular smooth muscle tone (reviewed by Vanhoutte, 1987; Fanburg, 1988). This important function has stimulated interest in the electrophysiologic properties of endothelial cells. A variety of ion channels have been reported in endothelial cells, including nonselective receptor-operated currents (Johns et al., 1987; Bakhramov et al., 1988), a nonselec-

tive cation channel (Fichtner et al., 1987), a stretch-activated cation channel (Lansman et al., 1987), a shear stress-activated K^+ current (Olesen et al., 1988a), A currents (Takeda et al., 1987), an acetylcholine-activated K^+ channel (Olesen et al., 1988b), Ca-activated K^+ channels (Colden-Standfield et al., 1987; Fichtner et al., 1987; Sauve et al., 1988), and inward rectifier K^+ channels (Colden-Stanfield et al., 1987; Johns et al., 1987; Takeda et al., 1987; Silver et al., 1987; Olesen et al., 1988b). In all whole-cell studies of endothelial cells, the predominant ion channel is the inward rectifier (IR). One function of the IR in endothelial cells is to maintain the resting membrane potential, as IR blockers depolarize the membrane (Johns et al., 1987).

It has been suggested that inward rectification could result from voltage-dependent block by an intracellular blocking particle (Armstrong and Binstock, 1965; Hagiwara and Takahashi, 1974). This possibility has been explored further by detailed modeling (Armstrong, 1975; Hille and Schwarz, 1978; Standen and Stanfield, 1978a). It was recently reported that internal Mg^{2+} is a potent time- and voltage-dependent blocker of outward IR currents in cardiac myocytes (Matsuda et al., 1987; Vandenberg, 1987; Matsuda, 1988; Saigusa and Matsuda, 1988). These observations raise the possibility that IR channels might not have an intrinsic gating mechanism; that some or all of the observed inward rectification may be due to block of outward currents by physiological levels of internal Mg^{2+}. In the present study, the voltage, $[K^+]_o$, and time dependence of IR gating in endothelial cells are described with high (~1.9 mM) and low ($\leq$20 nM) free Mg^{2+} in the pipette solution. Comparison of these properties of the IR in cells with nominally Mg-free internal solutions and in cells with $[Mg^{2+}]_i$ near or above physiological levels reveals only subtle differences. Although the $[Mg^{2+}]$ just inside the membrane is not known precisely, the similarity of gating under these two conditions suggest that inward rectification in endothelial cells is largely due to an intrinsic gating mechanism.

This work has been presented in abstract form (Silver et al., 1987; Silver and DeCoursey, 1989).

METHODS

Endothelial Cell Isolation

Bovine pulmonary artery endothelial cells were isolated by enzymatic digestion as described by Rubin et al. (1984) from fresh bovine heart-lung preparations obtained from a slaughterhouse. The main pulmonary arteries were isolated, incubated for 15 min in ice-cold, Krebs-Ringer bicarbonate buffer (KRBB) containing (in millimolar): 120 NaCl, 4 KCl, 1.2 KH_2PO_4, 1.2 $MgSO_4$, 1.2 $CaCl_2$, 24 $NaHCO_3$, 4 glucose, and rinsed with sterile Ca- and Mg-free Hank's balanced salt solution (Gibco Laboratories, Grand Island, NY) containing 1% antibiotics (10,000 U/ml streptomycin and 10,000 μg/ml penicillin, Gibco). One end of the vessel was occluded, and then the vessel was distended with KRBB containing 0.25% collagenase (Worthington CL-II; Cooper Biomedical, Malvern, PA) and incubated for 30 min at 37°C. The cell-enzyme suspension was collected and combined with cells obtained by rinsing the pulmonary artery with KRBB. The fluid was centrifuged at 1,000 g for 10 min at 4°C and the supernatant was discarded. The remaining pellet was resuspended in a solution of RPMI 1640, 1% L-glutamine, 1% antibiotics, and 10% fetal calf serum (FCS) (all from Gibco). Cells

were plated at a density of 10^6 cells/dish in sterile T-25 tissue culture flasks (Falcon, Lincoln Park, NJ).

Cells were passaged by rinsing the flasks with Ca-free and Mg-free Hanks balanced salt solution. Three ml of 0.05% trypsin-0.53 mM EDTA (Gibco) were then introduced, the flask was swirled, and the trypsin-EDTA was removed. After ~30 s, medium containing 10% FCS was added to the flask, the contents were mixed, and cells were plated at 5×10^5 cells/flask in a different T-25 flask.

TABLE I
Composition of Solutions (in Millimolar)

	Extracellular (bath) solutions						
	Na^+	K^+	Ca^{2+}	Mg^{2+}	Cl^-	HEPES	V_{jct}
							mV
Ringer	160	4.5	2	1	170.5	5	—
10 K Ringer	150	10	2	1	166	5	0.8
20 K Ringer	140	20	2	1	166	5	1.1
40 K Ringer	120	40	2	1	166	5	1.6
80 K Ringer	80	80	2	1	166	5	2.6
160 K Ringer	0	160	2	1	166	5	4.6

	Intracellular (pipette) solutions										
Solution	K^+	Ca^{2+}	Mg^{2+}	Cl^-	F^-	$CH_3SO_3^-$	EDTA	EGTA	V_{jct}	$[Ca^{2+}]$	$[Mg^{2+}]$
									mV	nM	nM
1	160	2	—	4	—	120	10	10	10.5	14	20
2	160	1	2	6	—	140	—	10	10.5	85	1.9×10^6
3	162	1	2	6	140	—	—	11	9.0	8	4
4	162	1	2	146	—	—	—	11	4.6	85	1.9×10^6
5	162	1	2	73	70	—	—	11	6.7	36	18
6	162	5	—	—	162	—	—	—	9.0	6	3

Values for junction potentials, V_{jct}, were calculated as described in the Methods. The values of V_{jct} for intracellular solutions vs. Ringer are subtracted from the nominal potential to correct for the V_{jct} arising between the pipette solution and the bath at the beginning of each experiment. Values for V_{jct} for external solutions are added to nominal potentials to correct for the V_{jct} arising between a given bath solution and Ringer in the bath electrode. The pH of internal solutions was adjusted to 7.2 with KOH and external solutions to 7.4 with NaOH. EGTA, ethyleneglycol bis (β-aminoethyl ether)-N,N,N',N'-tetraacetic acid; EDTA, ethylenediamine-tetraacetic acid; and HEPES, 4-(2-hydroxyethyl)-1-piperazineethanesulfonic acid. The dipotassium salt of EGTA was used. For the purpose of calculating free divalent concentrations, the deionized water used for making all solutions was assumed to contain 15 μM Ca^{2+} and 30 μM Mg^{2+}. For solutions containing F^-, free divalent concentrations are based on solubility product constants from Weast (1987). Solutions with ≤ 20 nM Mg^{2+} (1, 3, 5, and 6) are referred to as 0 $mM[Mg^{2+}]$, or Mg-free. Internal solutions 1–5 also contain 10 mM HEPES, solution 6 contains 5 mM HEPES and 5 mM ATP (as CaATP). Most experiments were done with solutions 1 and 2.

For electrophysiologic studies, cells from the initial or subsequent passage were plated at a density from 2–10 $\times$ 10^4 cells/dish in 35-mm tissue culture dishes containing several small pieces of sterile glass coverslips. All cells were incubated in 5% CO_2-air at 37°C. A piece of coverslip with adherent cells was transferred to a small recording chamber and perfused with Ringer's solution (Table I). Cells were studied after the initial isolation and from the third to tenth passage. In preliminary studies, IR channels were found in preconfluent round and elongated cells, and in flattened cells in confluent monolayers. To minimize space-clamp

errors, for this study we recorded from rounded, preconfluent cells. A sample of 25 cells had an input capacitance of 10.4 ± 3.5 pF (mean $\pm$ SD).

Identification of bovine pulmonary artery endothelial cells. Endothelial cells were identified by several criteria. Firstly, endothelial cells exhibit a contact-inhibited growth pattern giving rise to a "cobblestone" appearance at confluency (Ryan et al., 1978a). Secondly, the cultures had a high level of angiotensin-converting enzyme activity, assessed by measuring the hydrolysis of [^{3}H]benzoyl-Phe-Ala-Pro (Ventrex Laboratories, Portland, ME) (Ryan et al., 1978b). Finally, 95% of cells from the initial isolation demonstrated factor VIII-related antigen (Jaffe et al., 1973) when assayed between the third and sixth passages. The remaining 5% may have been endothelial cells without factor VIII-related antigen or contaminating fibroblasts.

Recording Techniques

Whole-cell voltage-clamp was done using GΩ-seal technique. Micropipettes were pulled in several stages from 7052, EG-12 or 0010 glass (Garner Glass Co., Claremont, CA), coated with Sylgard 184 (Dow Corning Corp., Midland, MI), and heat polished to a pipette tip resistance measured in Ringer's solution of 2–5 MΩ. These glass types have low intrinsic noise (Rae and Levis, 1984) and formed tight seals (10–50 GΩ) with endothelial cell membranes. Most pipette solutions used contained 10 or 11 mM EGTA (Table I), which is sufficient to chelate heavy metals which may be released from the pipette glass (Cota and Armstrong, 1988; Furman and Tanaka, 1988). A reference electrode made from a Ag-AgCl pellet was connected to the bath through an agar bridge saturated with our standard bath solution, Ringer. Signals were fed through the patch clamp (Axopatch-1A; Axon Instruments, Inc., Burlingame, CA, or List Patch Clamp L/M-EPC 7, Medical Systems Corp., Great Neck, NY), into an Indec Data Acquisition System (Indec Corp., Sunnyvale, CA) for storage and analysis. To resolve the gating kinetics of IR currents, capacity compensation was critical and was adjusted before each run. Capacity transients were cancelled for voltage steps between potentials positive to E_K at which IR channels were largely closed. In some experiments, careful nulling of the capacity at positive potentials where the input resistance of the cell was high, resulted in distorted current waveforms for hyperpolarizing pulses to potentials where the input resistance of the cell was low. This phenomenon is probably due to the dependence of the capacity time constant on the input resistance of the cell (which changes instantaneously [see Results]) under conditions when the input resistance is not infinitely larger than the pipette resistance, as discussed by Tessier-Lavigne et al. (1988). After adjusting the capacity compensation, the series resistance compensation was set as high as possible without ringing. All experiments were conducted at room temperature, 20–23°C.

Absolute potentials were established at the start of each experiment by defining 0 mV as the zero current potential with the pipette in the bath in Ringer's solution. Data were corrected for the junction potentials as described in Table I. Junction potentials were calculated using the Henderson (1907) equation using mobility and activity coefficients from Robinson and Stokes (1965), Weast (1987), and Landolt-Börnstein (1960). Apparent binding constants for EDTA, EGTA, and ATP were derived from Martell and Smith (1974).

Buffering of Internal Magnesium

Although there is ample evidence that rapid exchange between the pipette solution and the cytoplasm takes place in small spherical cells in the whole-cell configuration (Marty and Neher, 1983; Pusch and Neher, 1989), the importance of this assumption for the present study led us to attempt to confirm directly that the IR channels in endothelial cells "see" the pipette solution. Fig. 1 A illustrates whole-cell currents during voltage ramps after various times in the whole-cell configuration with a K-free pipette solution (major cation N-methylglucamine,

NMG$^+$, see legend). Within seconds after breaking into the cell, the outward current observable initially disappears, making the reversal potential, V_{rev}, unmeasurable. The inward current at this time is not much affected, so it would appear that the disappearance of outward current reflects a positive shift of V_{rev} with little immediate change in the voltage dependence of IR gating. The maximum slope conductance decreased over the first minute after achieving whole-cell configuration, with a time course illustrated in Fig. 1 *B*. The slope conductance decreased to a value roughly 50% of the initial value, with a time constant of <1
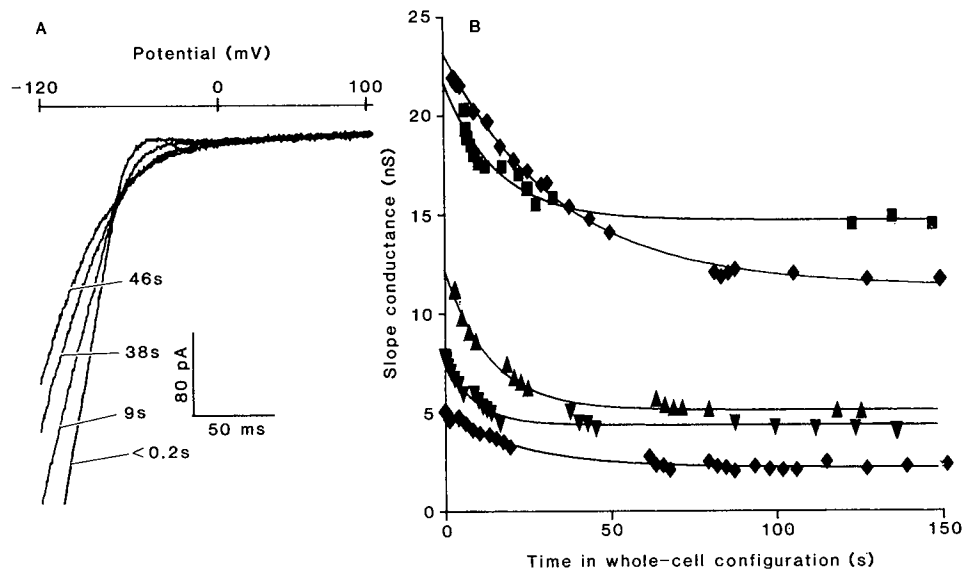
FIGURE 1. Time course of changes in IR currents after achieving whole-cell configuration with a K-free pipette solution (120 mM NMG$^+$, 100 mM NO$_3^-$, 20 mM Cl$^-$, 5 mM HEPES, 10 mM EGTA, pH 7.2), and Ringer in the bath. (*A*) Superimposed currents during voltage ramps from a cell (also shown in *B* as ▼) immediately after breaking into the cell and 9, 38, and 46 s after achieving whole-cell configuration. The cell was ramped repeatedly from −120 to 100 mV over 200 ms. There has been no junction potential correction. The horizontal axis does not represent zero current; these records all have an identical vertical offset because cell capacity was not compensated. (*B*) The decrease in maximum slope conductance with time after breaking into the cell with the K-free pipette solution described in *A* is shown for five cells. The data for each cell are fit with single exponential curves. For each cell the amplitude, time constant, and steady-state conductance, as well as the input capacity and pipette resistance (measured in the bath) are: (♦) 11.9 nS, 35 s, 11.3 nS, 22 pF, 5.2 MΩ; (■) 7.0 nS, 15.9 s, 14.7 nS, 21 pF, 2 MΩ; (▲) 7.1 nS, 13.8 s, 5.1 nS, 14 pF, 3.6 MΩ; (▼) 3.4 nS, 9.0 s, 4.3 nS, 15.4 pF, 3.6 MΩ; and (♦) 2.9 nS, 23.5 s, 2.2 nS, 9 pF, 4.6 MΩ.

min for a variety of cell sizes and pipette resistances. Assuming that the decreased conductance reflects replacement of K$^+$ by NMG$^+$, there do not appear to be significant or unexpected barriers to diffusion in endothelial cells. That the IR conductance is not abolished (as would be predicted by extrapolation of the dependence of the IR conductance on the geometric mean of [K$^+$]$_o$ and [K$^+$]$_i$ found by Hagiwara and Yoshii [1979] in egg cells at higher [K$^+$]$_o$ and [K$^+$]$_i$ than used here) is not surprising: Na$^+$ and Ca^{2+} channels carry large inward currents with Na-free or Ca-free internal solutions, respectively, delayed rectifier channels

carry outward K^+ currents into a K-free bath, and Mitra and Morad (1987) observed inward IR currents after replacement of $[K^+]_i$ by NMG^+.

The time constants for the five experiments in Fig. 1 are 9–35 s, similar to the time constants of diffusional equilibration predicted by empirical equations given by Pusch and Neher (1988). The predicted time constants of equilibration for EDTA (solution 1, Table I) or ATP, (solution 6, Table I) ranges 0.3–3 min for typical spherical endothelial cell sizes, pipette resistances, and assuming a doubling of pipette resistance in whole-cell configuration compared with pipette resistance in the bath. After one time constant, the cell would contain ~7 mM EDTA, which would buffer 2 mM free cytoplasmic Mg^{2+} to 3 μM. Most recent estimates of $[Mg^{2+}]_i$ are <1 mM in frog muscle (Godt and Maughan, 1988), rat hepatocytes (Raju et al., 1989), chicken heart (Murphy et al., 1989), and ferret ventricle (Blatter and McGuigan, 1986). As MgEDTA diffuses into the pipette, $[Mg^{2+}]_i$ will approach that in the pipette solution, ~20 nM. In a number of experiments, free Mg^{2+} was buffered by F^- in the pipette (solutions 3, 5, and 6, Table I). Small anions like F^- would be expected to diffuse rapidly into the cell (Marty and Neher, 1983). Since MgF_2 has a very low solubility (Weast, 1987), $[Mg^{2+}]_i$ would approach 3 nM. The only consistent difference found between cells studied with F^- compared with cells with $CH_3SO_3^-$ in the pipette solution was that the leak current was usually larger with F^-; kinetic parameters of IR currents were the same. In a few experiments, free Mg^{2+} was buffered with ATP (solution 6, Table I), with similar results. In summary, equilibration of our pipette solutions is probably complete within the first few minutes of each experiment.

If Mg^{2+} had a finite membrane permeability, or was in some way transported across the cell membrane, then it is conceivable that the $[Mg^{2+}]$ just inside the membrane might be higher than the bulk $[Mg^{2+}]_i$. Mathias et al. (1989) have shown that including membrane permeability reduces the time required for bulk equilibration of cytoplasm and pipette solutions. In order to estimate the $[Mg^{2+}]_i$ just under the membrane, we have applied a compartmental diffusion model analagous to that described by Hille (1977). We assumed a cell diameter of 10 μm, a pipette tip diameter of 1 μm, a diffusion coefficient of 0.71 × 10^{-5} cm^2/s (Weast, 1987), and a membrane permeability of 0.07 × 10^{-6} cm/s determined in barnacle muscle cells (Montes et al., 1989). With initial concentrations of 2 mM Mg^{2+} in the bath, 10 mM Mg^{2+} in the cellular compartments and 0 mM Mg^{2+} in the pipette, the model predicts that $[Mg^{2+}]_i$ in the compartment just inside the membrane would drop with a time constant of 2.3 s to 1.9 μM even without considering the effects of Mg^{2+} buffers used. These calculations suggest that $[Mg^{2+}]_i$ will rapidly fall to a few micromolar simply by diffusing into the pipette; as Mg^{2+} buffers from the pipette enter the cell, free $[Mg^{2+}]_i$ will be further reduced.

RESULTS

In bovine pulmonary artery endothelial cells studied in whole-cell configuration, the membrane conductance is predominated by potassium currents resembling IR currents in other cells. Infrequently, whole-cell currents were seen that closely resembled "A" currents described in nerve (Conner and Stevens, 1971; Neher, 1971). A currents were detected less frequently in bovine pulmonary artery endothelial cells than they were reported in bovine aortic endothelial cells where they are present in approximately one-third of the cells (Takeda et al., 1987). Fig. 2 A illustrates a family of whole-cell voltage-clamp current records in an endothelial cell bathed in Ringer's solution containing 4.5 mM K^+ (Table I). Depolarization elicits only small outward currents, while hyperpolarizing voltage steps give rise to large inward currents. The endothelial cell membrane behaves as an IR, conducting large

inward currents at potentials negative to the potassium reversal potential, E_K, but only small outward currents positive to E_K. The inward currents increase during the first few milliseconds after a hyperpolarizing voltage pulse. This time dependence is the result of activation, or opening of closed channels, which occurs more rapidly at more negative potentials.

During large hyperpolarizing pulses (Fig. 2 *A*), the inward currents rise rapidly and then decay with time. This decay is faster and more complete at more negative potentials, thus resembling voltage-dependent block by external Na^+ as has been demonstrated for IR currents in other cells (Ohmori, 1978; Standen and Stanfield, 1979). Consistent with the mechanism of Na^+ block, the rapid decay was abolished
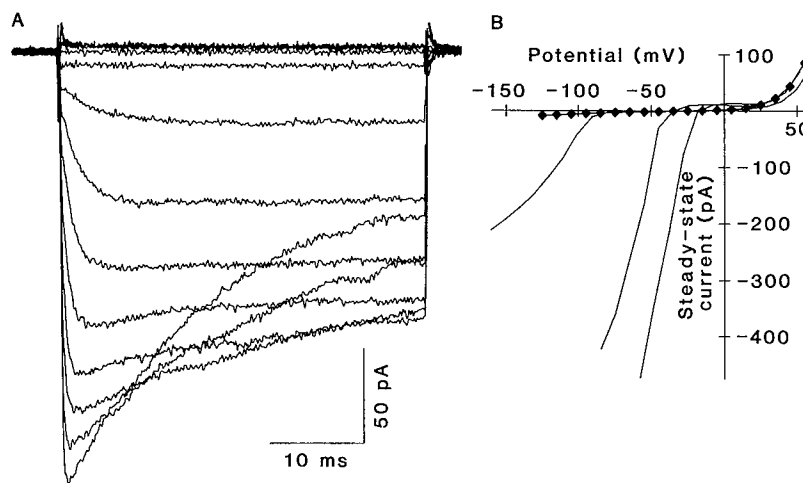

FIGURE 2.   (*A*) Whole-cell IR currents in a cell in 4.5 K^+ Ringer with a Mg-free pipette solution (solution 1, Table I). From a holding potential of -79 mV, pulses to potentials ranging from -169 to -39 mV in 10-mV steps were applied every 1.5 s. (*B*) Steady-state current-voltage relationship of the IR in several solutions are shown without leak correction. Steady-state outward currents and peak inward currents from Fig. 2 *A* as well as currents in the same cell in 40 K^+ Ringer and 80 K^+ Ringer are shown with data points connected by lines. The currents reverse at more positive potentials as $[K^+]_o$ is increased. 10 mM Ba^{2+} added to 40 K^+ Ringer (♦) blocks both inward and outward currents through the IR.

by replacement of Na^+ by TMA^+ (data not shown) and became less pronounced as $[K^+]_o$ was increased. Even in 160 mM $[K^+]_o$, or with all external Na^+ replaced by TMA^+, there was still a small decay of current, much slower than with Na^+ present. Whether this slower decay is due to block by external divalent cations (cf. Biermans et al., 1987) or to an intrinsic inactivation mechanism was not determined.

When $[K^+]_o$ is increased to 40 or 80 mM $[K^+]_o$ (Fig. 2 *B*), the currents reverse at more positive potentials, always near E_K. As $[K^+]_o$ increases, the slope conductance of inward currents increases and the voltage range within which the potassium conductance is activated also shifts to more positive potentials. Both the large inward currents and the small outward currents are blockable by 10 mM Ba^{2+} (♦, Fig. 2 *B*),

a potent blocker of IR currents in other cells (Hagiwara et al., 1978; Standen and Stanfield, 1978b). At potentials positive to $+30$ mV in Fig. 2 B, the conductance increases. Neither Ba^{2+} nor changes in $[K^+]_o$ affect this increased conductance which was present to some extent in every cell studied. This conductance is therefore unrelated to IR, but interfered with the study of outward IR currents in high $[K^+]_o$ (80 or 160 mM).

Steady-state outward currents. At potentials positive to E_K, small steady-state outward currents can be seen in Fig. 2 B. In Fig. 3, steady-state currents from seven cells are plotted at much higher gain. To compare cells with 0 $[Mg^{2+}]_i$ (Fig. 3 A) and 1.9 mM $[Mg^{2+}]_i$ (Fig. 3 B), steady-state currents in Ringer's solution were normalized according to each cell's maximum slope conductance at negative potentials. This corrects for cell-to-cell variability in the whole-cell IR conductance. All of the cells in
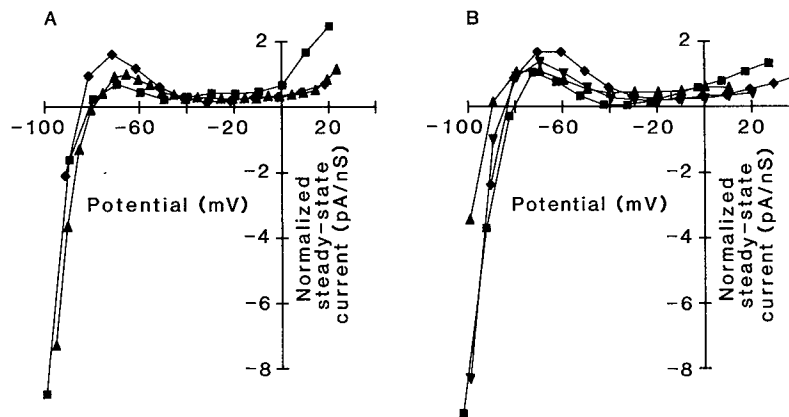

FIGURE 3. Steady-state current-voltage relation in three cells containing 0 $[Mg^{2+}]_i$ (A) and in four cells containing 1.9 mM $[Mg^{2+}]_i$ (B) with $CH_3SO_3^-$ as the main internal anion (pipette solutions 1 or 2, respectively). Steady-state outward currents and peak inward currents are plotted without leak correction. Currents were normalized by dividing by the maximum slope conductance in each cell at potentials at which the IR conductance was maximally activated.

Fig. 3 contained similar internal solutions with $CH_3SO_3^-$ as the main anion (1 and 2, Table I), and differ only in Mg^{2+} and EDTA. Regardless of $[Mg^{2+}]_i$, in all cells there were large inward currents, a small bump of outward current and a negative slope conductance region. The outward currents at quite positive potentials (positive to 0 mV), as discussed above, appear to be unrelated to IR. The magnitude of the outward current bump and negative slope conductance region appears similar in cells with and without $[Mg^{2+}]_i$ although the outward currents appear to be present over a slightly broader voltage range in cells with high $[Mg^{2+}]_i$ (Fig. 3 B). The small absolute amplitude of the outward current and the nonlinearity of the leak conductance at positive potentials preclude more quantitative comparison. In general, steady-state outward current through the IR became undetectable more than 40–60 mV positive to E_K. Steady-state outward current was seen at all $[K^+]_o$ from 4.5 to 160 mM.

Voltage Dependence of Activation

IR channels open upon hyperpolarization and close on depolarization. To quantify the voltage dependence of channel gating, we used a protocol illustrated in the insets to Fig. 4. Prepulses to various potentials were given, followed by a step to a constant test potential at which activation or deactivation kinetics were resolvable. The instantaneous current, I_0, at the beginning of the test pulse is directly proportional to the fraction of IR channels open at the end of each prepulse. I_0 was obtained by fitting the current transient with a single exponential function:

$$I_K(t) = (I_0 - I_\infty) \exp(-t/\tau) + I_\infty, \tag{1}$$

where $I_K(t)$ is the current at any given time, I_0 is the instantaneous current, I_∞ is the steady-state current, the τ is the time constant of activation or deactivation. As can be seen in the insets, a large negative prepulse opens IR channels maximally, so that I_0 at the beginning of the test potential is maximal. In these examples, the IR conductance was not maximally activated at the test potential, so the test current decays somewhat after a very negative prepulse. After a depolarizing prepulse I_0 is small and the test current increases with time as channels open during the test pulse. At a given test potential, activation and deactivation had the same time constant and the same steady-state current, consistent with a first-order C $\rightleftarrows$ O process. Normalized values of I_0 are plotted against prepulse potential for several different $[K^+]_o$ for a cell with 0 $[Mg^{2+}]_i$ (Fig. 4 A) and for another cell with 1.9 mM $[Mg^{2+}]_i$ (Fig. 4 B). A number of points can be made: (a) voltage-dependent gating is clearly present in all cells with or without internal Mg^{2+}; (b) regardless of $[Mg^{2+}]_i$, the voltage dependence of gating shifts along with E_K (observed V_{rev} values in each solution are indicated by bars on the voltage axis) to more positive potentials as $[K^+]_o$ increases; (c) the voltage dependence of IR channel gating is steep, and (d) even after careful leak subtraction, the values obtained for I_0 do not always limit to 0.

The relationship between I_0 and the prepulse potential, V, was quantified by fitting the data by nonlinear least squares with a Boltzmann function:

$$I_0(V) = \frac{I_{0,max} - I_{0,min}}{1 + \exp[(V - V_n)/k_n]} + I_{0,min} \tag{2}$$

and adjusting the minimum and maximum instantaneous currents at the test potential, $I_{0,min}$ and $I_{0,max}$, respectively, the half-activation potential V_n, and the slope factor k_n, which expresses the steepness of the voltage dependence. The steady-state voltage dependence of activation from a number of experiments like those in Fig. 4 is summarized in Table II. To allow comparisons in different $[K^+]_o$, the difference between the absolute potential at the midpoint of the activation curve, V_n, and the observed reversal potential, V_K, is given. The midpoint of the activation curve was consistently negative to V_K by about the same amount in all $[K^+]_o$. Thus, as is characteristic of IR in other cells, as $[K^+]_o$ is changed, the voltage dependence of IR gating shifts along with E_K. $V_n - V_K$ was similar in cells with and without $[Mg^{2+}]_i$ at all $[K^+]_o$. The voltage dependence of steady-state activation (k_n in Table II) is quite steep, averaging 4.3 mV in 0 $[Mg^{2+}]_i$ and 5.2 mV in 1.9 mM $[Mg^{2+}]_i$. These slope factors correspond to 5.9 and 4.9 gating charges, respectively, moving across the
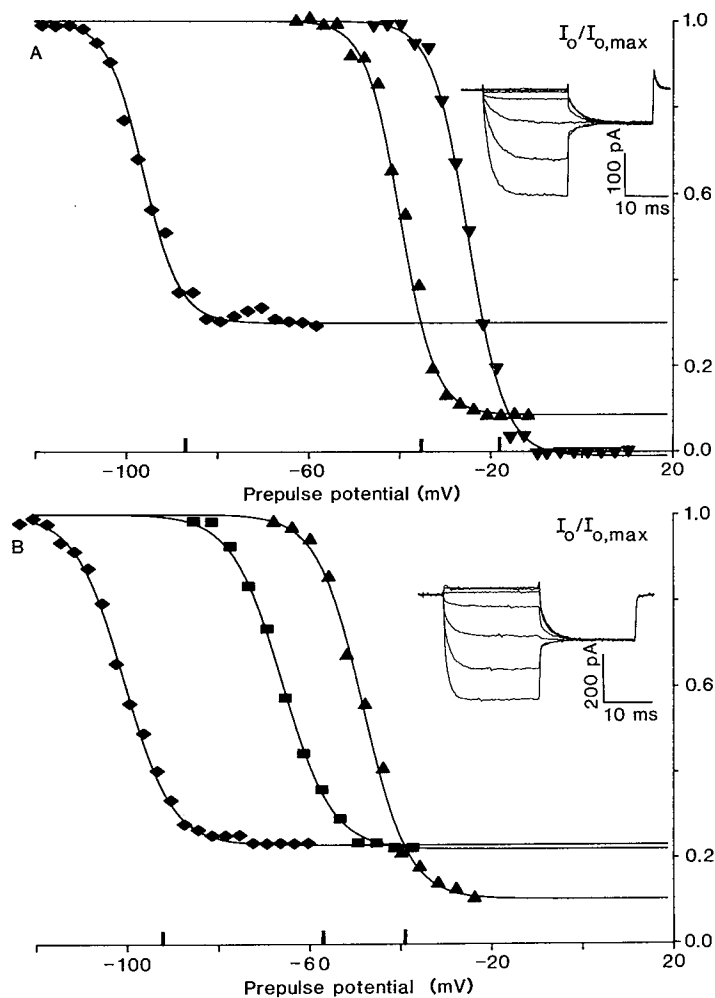
FIGURE 4. Steady-state voltage dependence of IR gating in a cell with (A) 0 $[\mathrm{Mg}^{2+}]_i$ or (B) 1.9 mM $[\mathrm{Mg}^{2+}]_i$. (A) Activation curves from a cell containing solution 1 bathed in Ringer (◆), 40 K^+ Ringer (▲), or 80 K^+ Ringer (▼). Inset illustrates the measurement in 80 K^+ Ringer. The cell was held at -8 mV and stepped for 20 ms to potentials ranging from -40 to 2 mV in 6-mV increments, then stepped to a constant test potential (-28 mV), with 3 s between pulses. The instantaneous current at the beginning of the test pulse was determined by extrapolating to time zero a single exponential fitted to the current relaxation. The instantaneous currents were leak corrected, fit with a Boltzmann (Eq. 2) and plotted against the prepulse potential. Fitted parameters used to draw the curves are: $V_n = -97$ mV, $k_n = 4.6$ mV (◆); $V_n = -39$ mV, $k_n = 3.8$ mV (▲); and $V_n = -25$ mV, $k_n = 3.9$ mV (▼). Bars on the voltage axis show V_{rev} observed in each solution. (B) Activation curves from a cell containing solution 2 in Ringer (◆), 20 K^+ Ringer (■), or 40 K^+ Ringer (▲). Inset illustrates the measurement in 20 K^+ Ringer, where the cell was held at -58 mV and stepped for 20 ms to potentials ranging from -89 to -33 mV in 8-mV increments, followed by a step to a constant test potential (-74 mV). Fitted parameters are $V_n = -101$ mV, $k_n = 5.0$ mV (◆); $V_n = -66$ mV, $k_n = 5.6$ mV (■); and $V_n = -48$ mV, $k_n = 5.1$ mV (▲).

entire membrane field. The difference between k_n in cells studied with 0 $[Mg^{2+}]_i$ and 1.9 mM $[Mg^{2+}]_i$ is statistically significant. Changing $[K^+]_o$ had no effect on k_n.

We attempted to detect the steepening of the voltage dependence indicated by the k_n values in Table II in several cells after achieving whole-cell configuration with a Mg-free pipette solution. The first activation curve measurement could be completed only ~3 min after breaking into the cell because of the time required to carefully cancel capacity transients and to establish and carry out the pulse protocol. Activation curves determined over the next 30 min were not detectably different. Apparently, $[Mg^{2+}]_i$ is reduced by equilibration with Mg-free pipette solutions within the first few minutes after achieving whole-cell configuration, as indicated in Fig. 1, so that k_n had already decreased before the measurement of the first activation curve.

TABLE II
Steady-State Voltage Dependence of IR

	$[Mg^{2+}]_i = 0$			$[Mg^{2+}]_i = 1.9$ mM		
$[K^+]_o$	$V_n - V_K$	k_n	n	$V_n - V_K$	k_n	n
mM	*mV*	*mV*		*mV*	*mV*	
4.5	−9.3	4.2	13	−9.3	4.9	13
10	−5.4	4.5	5	—	—	—
20	−5.2	4.5	6	−7.4	4.3	4
40	−8.1	4.1	11	−5.4	5.2	7
80	−6.9	4.6	5	−8.6	5.2	2
160	−4.2	4.1	5	−7.8	6.3	5
All	−7.2	4.3	45	−7.9	5.2	31
±SE	±0.7	±0.1		±0.8	±0.2	

Steady-state voltage dependence of IR gating derived from activation curves as described in Fig. 4 and in the text. The difference between the midpoint of the activation curve, V_n (Eq. 2, see text) and the reversal potential, V_K, observed in each experiment is given as $V_n - V_K$. The difference between the combined values for $V_n - V_K$ in cells with or without internal Mg^{2+} were not different ($P > 0.4$ by student's t test). The slope factor, k_n, was significantly smaller in cells with 0 $[Mg^{2+}]_i$ ($P < 0.005$).

If all channels are closed after a strong depolarizing prepulse, the instantaneous current during a hyperpolarizing voltage step should equal the "leak" current, or current not flowing through IR. However, when this pulse protocol was used (Fig. 4), the instantaneous current was often larger than could be explained on the basis of leak or non-IR current. Even though all currents in Fig. 4 were leak corrected, several of the curves in Fig. 4 limit to a nonzero value, $I_{0,min}$. This additional current was observed consistently in cells containing 1.9 mM $[Mg^{2+}]_i$ and averaged 0.31 ± 0.01 (mean ± SE, $n = 25$) of the total IR current over all $[K^+]_o$. As a control for the possibility that the prepulses used were not long enough to reach steady state (cf. Leech and Stanfield, 1981), in some cells the prepulse duration was increased to several minutes; the activation curve still had a nonzero limit. Addition of Ba^{2+} eliminated both time-dependent and instantaneous IR currents (data not shown). In cells with 0 $[Mg^{2+}]_i$, $I_{0,min}$ tended to be smaller, especially at higher $[K^+]_o$, averaging

0.14 ± 0.02 (mean ± SE, $n = 32$) over all $[K^+]_o$. The difference between $I_{0,min}$ with 0 $[Mg^{2+}]_i$ or 1.9 mM $[Mg^{2+}]_i$ is significant ($P < 0.005$).

Instantaneous current-voltage relationships. In addition to steady-state outward current through IR (Fig. 3), deactivating outward current transients were observed when the IR was first activated by a hyperpolarizing prepulse, shown in the insets in Fig. 5 for cells without (Fig. 5 A) and with (Fig. 5 B) internal Mg^{2+}. Instantaneous current-voltage relationships (*I*-Vs) can therefore be compared in cells without $[Mg^{2+}]_i$ (Fig. 5 A) or with 1.9 mM $[Mg^{2+}]_i$ (Fig. 5 B). Plotted are instantaneous *I*-Vs for several cells in which the most reliable data were obtained, in 4.5 K^+ and 40 K^+
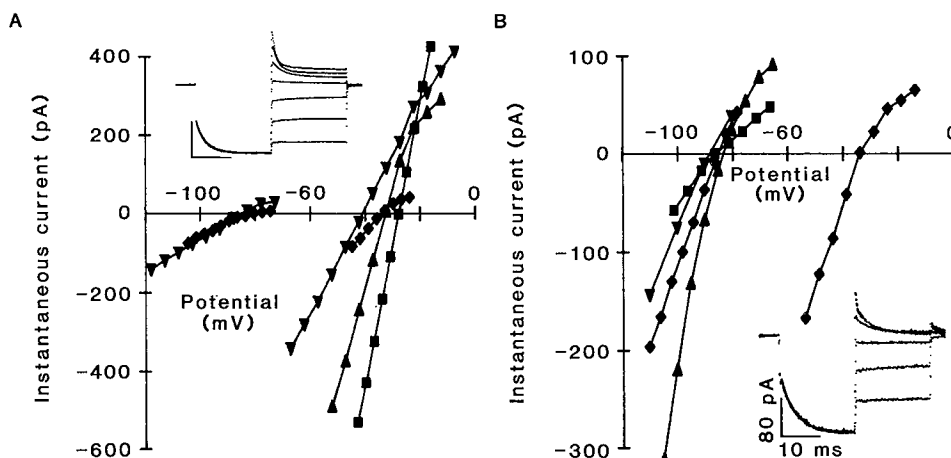

FIGURE 5.   Instantaneous current-voltage relationships in cells with (A) 0 $[Mg^{2+}]_i$ and with (B) 1.9 mM $[Mg^{2+}]_i$. All currents are shown without leak correction, and with different symbols for different cells. (A) Instantaneous current-voltage relationships for three cells in 4.5 K^+ Ringer and four cells in 40 K^+ Ringer. The inset illustrates the measurement in a cell in 40 K^+ Ringer, which was held at -29 mV, stepped to -49 mV to open IR channels and then stepped to various test potentials (-46 mV to -10 mV in 6-mV increments). For depolarizing pulses, a single exponential curve was fit to the deactivating currents to determine the current at the beginning of the test pulse. Calibration bars indicate 200 pA and 10 ms. (B) Instantaneous current-voltage relationships for four cells in 4.5 K^+ Ringer and one cell in 40 K^+ Ringer. The inset shows currents in a cell containing 1.9 mM $[Mg^{2+}]_i$ in 4.5 K^+ Ringer (♦), held at -80 mV, stepped to -110 mV to open IR channels and then to various test potentials (-102 mV to -78 mV in 8-mV increments).

Ringer. The instantaneous current was measured directly at voltages near or negative to E_K, and at positive potentials by fitting a single exponential to the outward current transients and extrapolating to the time at the start of the test pulse. Deactivation at potentials $>\sim 20$ mV positive to E_K was too rapid to permit accurate determination of the instantaneous current. Close to E_K, the instantaneous *I*-V is approximately linear. At more positive potentials there is in most cells a decreased conductance, or inward rectification. We are unsure whether this reflects the limits of the measurement or whether internal Mg^{2+} may have an effect; the instantaneous *I*-V with Mg-free

internal solutions sometimes appears to rectify as well. These data do not permit us to exclude the possibility of instantaneous rectification due to rapid block by internal Mg^{2+}, especially at potentials well positive to E_K. The presence of distinct outward currents with 1.9 mM $[Mg^{2+}]_i$ indicates that if rapid block does occur it is not complete. The question whether the decay of outward currents is due to deactivation or time-dependent block is addressed in the next section by comparing the voltage dependence of IR kinetics in cells with and without internal Mg^{2+}.

Deactivation kinetics. Deactivation or closing of open channels occurred rapidly at potentials positive to E_K in cells with and without internal Mg^{2+}. To confirm that outward current transients like those in the insets of Fig. 5 were due to deactivation
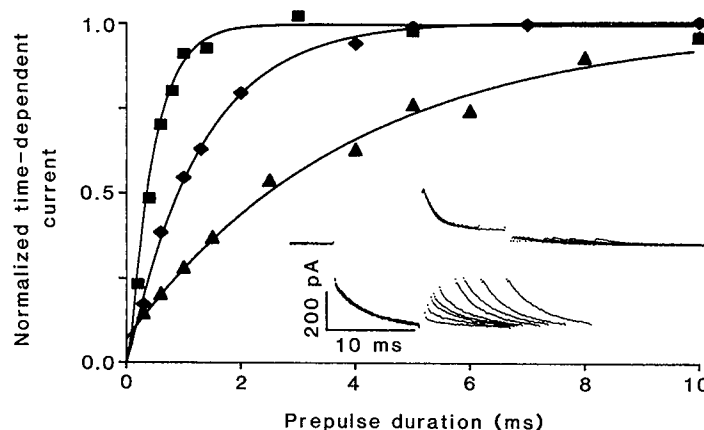

FIGURE 6.   The "envelope" method for obtaining deactivation time constants is illustrated in the inset in a cell containing solution 1, bathed in 40 mM K^+ Ringer. From a holding potential of -29 mV, a negative prepulse to -44 mV was given to open channels followed by a step to the test potential (-19 mV) for a variable duration, and then the potential was stepped back to the prepulse potential (-44 mV). The graph shows the amplitude of the time-dependent (activating) current during the second pulse to -44 mV plotted as a function of the test pulse duration for test potentials of -9 mV (■), -19 mV (♦), and -29 mV (▲). The curves show the best-fitting single exponential with τ's of 0.43 ms at -9 mV, 1.3 ms at -19 mV and 4.0 ms at -29 mV. Measured directly from the decay of outward current at -19 mV, τ was the same, 1.3 ms.

of IR channels and not capacity transients or another conductance, we used the protocol illustrated in the inset in Fig. 6. First, IR channels were opened with a hyperpolarizing pulse. The membrane was then stepped to a more positive test potential for a variable period of time, and then hyperpolarized again. The instantaneous current at the beginning of the second hyperpolarizing pulse, determined by fitting a single exponential curve to the activating current transient and extrapolating back to time zero, is proportional to the number of the channels open at the end of the depolarizing test pulse. As the duration of the depolarizing test pulse is increased, deactivation is more complete and the instantaneous current is reduced. The instantaneous currents during the second hyperpolarizing pulse form

an "envelope" whose time constant was similar to that measured directly from the outward current transient during the depolarizing pulse. At more positive potentials deactivation of IR currents was rapid and hard to distinguish from capacity transients, while the envelope method allowed determination over a slightly larger voltage range. We have therefore given much more weight to deactivation τ's determined by this method. The envelope method was also useful in determining deactivation τ's at potentials near E_K where current amplitudes are small. The amplitude of the time-dependent current ($I_0 - I_\infty$) is plotted in Fig. 6 for the test potential in the inset (◆, −19 mV). Analogous data for test potentials of −9 mV (■) and −29 mV (▲) show that deactivation is strongly voltage dependent, with τ decreasing by almost an order of magnitude over a 20-mV range.

Voltage dependence of activation and deactivation kinetics. Assuming a simple $C \rightleftarrows O$ model for channel gating, the rate constants for channel opening, α, and channel closing, β, can be determined from τ, where $\tau = 1/(\alpha + \beta)$, and the steady-state voltage dependence of activation, p_∞, where $p_\infty = \alpha/(\alpha + \beta)$. In Fig. 7, $1/\tau$ is plotted against voltage; τ was estimated for activation (▲) or deactivation (■) by directly fitting the current transients, and from deactivation envelopes (◆). To a first approximation, the rate constants, α (+) and β (×), determined in this way were both exponentially voltage dependent as indicated by the dotted lines in Fig. 7, A and C, which are drawn according to: $\alpha = \bar{\alpha} \exp [(V_n - V)/k_\alpha]$ and $\beta = \bar{\beta} \exp [(V - V_n)/k_\beta]$, where V_n is the midpoint of the activation curve determined during the same experiment by the method illustrated in Fig. 4, $\bar{\alpha}$ and $\bar{\beta}$, respectively, are the values of α and β at V_n, and k_α and k_β reflect the steepness of the voltage dependence of α and β. We used V_n as a reference point for both α and β because τ was largest near V_n in all solutions. While the values calculated for β fit an exponential voltage dependence fairly well, the values calculated for α at positive potentials often fell below the exponential voltage dependence obtained from data at more negative potentials (as in Fig. 7 A and C). Calculation of the rate constants is extremely sensitive to the p_∞-voltage relation because of its steepness. The observed deviations could result from a small underestimation of p_∞ at positive potentials (e.g., 0.01 instead of 0.02). Kurachi (1985) found that β was exponentially voltage dependent, but that α saturated at negative voltages.

In Fig. 7 B $1/\tau$-voltage relationships for the cell with 0 $[Mg^{2+}]_i$ in Fig. 7 A are plotted in 20, 40, 80, and 160 K^+ Ringer. Varying $[K^+]_o$ simply shifted the $1/\tau$-voltage relationship (*solid lines*) without clearly affecting $\bar{\alpha}$, $\bar{\beta}$, or the slope factors k_α and k_β. Determination of the kinetic parameters for a cell with 1.9 mM $[Mg^{2+}]_i$ is illustrated in Fig. 7 C. The $1/\tau$-voltage relationships obtained in 4.5, 20, and 40 K^+ Ringer in this cell are shown in Fig. 7 D.

The kinetic parameter values obtained for IR gating are summarized in Table III for cells with 0 $[Mg^{2+}]_i$ and cells with 1.9 mM $[Mg^{2+}]_i$ over a wide range of $[K^+]_o$. There is no consistent effect of $[K^+]_o$ on any of the parameters. There is no significant difference between any parameter with and without internal Mg^{2+}. If time- and voltage-dependent block by internal Mg^{2+} contributes to the time dependence of the observed IR current transients, then the kinetics of Mg^{2+} block must be similar to those of the intrinsic gating process at all $[K^+]_o$.
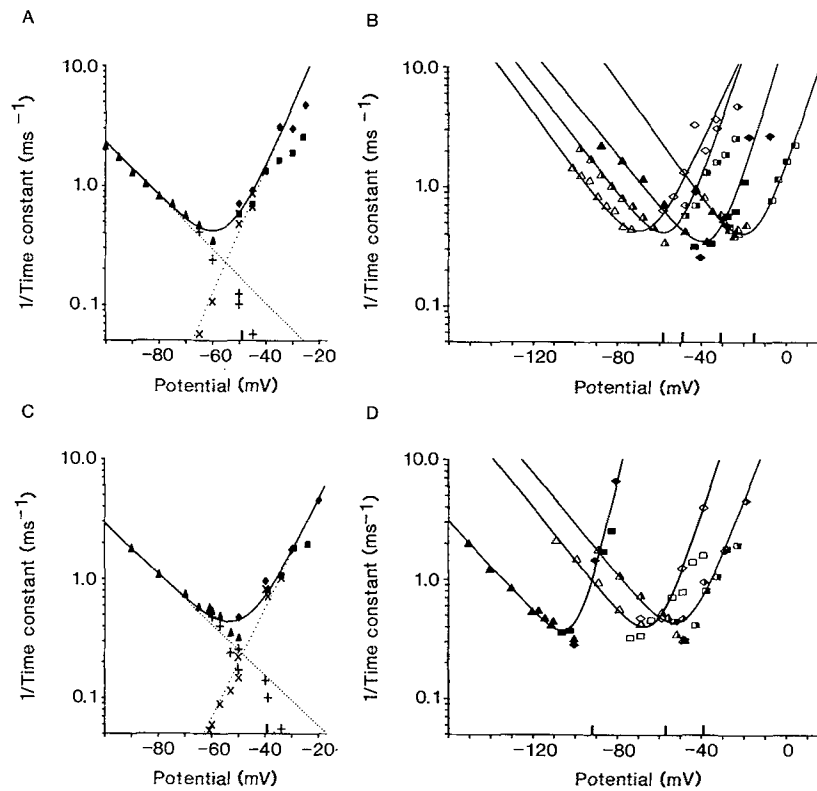
A

B

C

D

FIGURE 7. (A) $1/\tau$ is plotted against voltage for a cell in 40 K$^+$ Ringer with 0 [Mg^{2+}]$_i$ (solution 1). Activation τ's ($\blacktriangle$) were measured by fitting a single exponential to the rising current during hyperpolarizing voltage pulses, while deactivation τ's were determined either directly from the decay of the outward current ($\blacksquare$), or by the envelope method illustrated in Fig. 6 ($\blacklozenge$). Values of α (+) and β (x) were calculated as described in the text. The solid curve was fitted by eye to the $1/\tau$ data points, and is the sum of α and β, shown as the dotted lines. There was good agreement between deactivation τ's directly measured ($\blacksquare$) and τ's determined by the envelope method ($\blacklozenge$) near E_K. At more positive potentials, deactivation τ's measured directly tended to be larger than when determined by the envelope method. Deactivation τ's by the envelope method were given higher weight when fitting the curve. The observed V_{rev} in all parts is indicated by a bar on the voltage axis. (B) Fitted $1/\tau$ vs. voltage plots for the cell in A in 20, 40, 80, and 160 K$^+$ Ringer. Curves were fitted to $1/\tau$ data for each solution as shown in A, and with the same meaning of symbol shapes. The $1/\tau$-voltage relationship shifts to more positive potentials as [K$^+$]$_o$ increases. In 20 K$^+$ (*open symbols*), 40 K$^+$ (*right-half-filled symbols*), 80 K$^+$ (*filled symbols*), and 160 K$^+$ Ringer (*left-half-filled symbols*), respectively, $\bar{\alpha}$ was 0.25, 0.25, 0.23, 0.32 ms^{-1}; k_α was 18.4, 19.5, 20.5, 20.2 mV; $\bar{\beta}$ was 0.18, 0.18, 0.13, 0.12 ms^{-1}; and k_β was 11.4, 8.4, 7.6, 8.9 mV. For clarity the calculated α's and β's are omitted. (C) $1/\tau$ plotted against voltage for a cell with 1.9 mM [Mg^{2+}]$_i$ (solution 2) in 40 K$^+$ Ringer. Symbols are the same as in A. (D) Fitted $1/\tau$ vs. voltage plots for the cell in C in 4.5 K$^+$ (*filled symbols*), 20 K$^+$ (*open symbols*), and 40 K$^+$ Ringer (*right-half-filled symbols*). In 4.5, 20, and 40 K$^+$ Ringer, respectively, $\bar{\alpha}$ was 0.23, 0.28, and 0.26 ms^{-1}; k_α was 22.1, 20.2, 21.3 mV; $\bar{\beta}$ was 0.15, 0.13, 0.24 ms^{-1}; and k_β was 6.4, 8.1, 9.9 mV.

DISCUSSION

Is Internal Mg^{2+} the IR Gating Particle in Endothelial Cells?

The recent observation that the current-voltage relation of IR channels from guinea pig heart is linear in the absence of Mg^{2+} (Vandenberg, 1987; Matsuda et al., 1987) suggests the possibility that inward rectification might be largely or entirely the result of voltage- and time-dependent block by internal Mg^{2+}. Using whole-cell measure-

TABLE III

IR Rate Constants

$[K^+]_o$	n	$\bar{\alpha}$	k_α	n	$\bar{\beta}$	k_β
			$[Mg^{2+}]_i = 0$			
mM		ms^{-1}	mV		ms^{-1}	mV
4.5	10	0.19 ± 0.02	17.6 ± 1.1	9	0.09 ± 0.01	9.3 ± 0.4
10	3	0.18 ± 0.07	18.5 ± 4.5	3	0.10 ± 0.02	9.3 ± 1.0
20	4	0.18 ± 0.04	16.5 ± 2.4	4	0.11 ± 0.03	9.4 ± 0.8
40	10	0.21 ± 0.03	17.9 ± 1.4	9	0.09 ± 0.02	8.3 ± 0.7
80	4	0.20 ± 0.03	17.3 ± 1.7	4	0.10 ± 0.01	9.3 ± 1.4
160	3	0.24 ± 0.09	17.7 ± 2.4	3	0.09 ± 0.02	10.5 ± 1.1
All	34	0.203 ± 0.014	17.7 ± 0.71	32	0.097 ± 0.006	8.97 ± 0.31
			$[Mg^{2+}]_i = 1.9$ mM			
mM		ms^{-1}	mV		ms^{-1}	mV
4.5	9	0.15 ± 0.02	18.6 ± 1.2	7	0.09 ± 0.02	8.7 ± 0.9
20	3	0.22 ± 0.03	20.0 ± 1.2	3	0.09 ± 0.02	7.2 ± 1.0
40	5	0.18 ± 0.02	18.7 ± 1.5	5	0.08 ± 0.04	10.3 ± 1.3
80	1	0.33	31.4	1	0.10	6.9
160	1	0.14	20.0	—	—	—
All	19	0.175 ± 0.017	19.6 ± 0.96	16	0.091 ± 0.014	8.88 ± 0.67

Mean ± SE are given for n cells studied in each solution. The rate constants, α and β at a number of potentials were calculated as described in the text from parameters fitted to steady-state "activation curves" (Fig. 4) and from activation and deactivation τ's. Values for $1/\tau$ as well as the calculated rate constants were then fitted as shown in Fig. 7, to obtain values for $\bar{\alpha}$, $\bar{\beta}$, and for the slope factors k_α and k_β. In a few cells values for $\bar{\alpha}$ and k_α were estimated from activation data in the absence of deactivation data. Most of the data included in the table are from an experiment in which deactivation τ's were determined by the "envelope" method shown in Fig. 6; these estimates of τ were given more weight in fitting the data than τ derived by directly fitting outward current transients. There are no significant differences between the group means in cells with or without internal Mg^{2+} for any of the four parameters ($P > 0.1$).

ments, Matsuda et al. (1987) concluded that an intrinsic gating mechanism was also present at low $[Mg^{2+}]_i$; but these data were collected in the presence of 15 μM $[Mg^{2+}]_i$. In light of the half-block concentration of 1.7 μM Mg^{2+} at +70 mV reported by Matsuda (1988), the question arises whether what was interpreted as intrinsic gating might have been at least in part the result of block by residual Mg^{2+} (cf. Saigusa and Matsuda, 1988). Matsuda (1988) also reported intrinsic gating at the single-channel level using the open-cell attached-patch configuration, but the gating

kinetics slowed progressively during long experiments, as would be expected if the gating or blocking particle were gradually diffusing out of the ruptured cell. Based on these studies, the conclusion that inward rectification in cardiac muscle is largely due to internal Mg^{2+} block under physiological conditions seems better established than does the existence of an intrinsic gating mechanism. In the present study, the gating kinetics of IR channels in the presence and absence of internal Mg^{2+} were quantified and compared to test whether the IR of endothelial cells, which in most respects resembles that of other cells including cardiac muscle, also shares a high sensitivity to block by internal Mg^{2+}.

The main conclusion of this study is that IR channels in endothelial cells have a steeply voltage-dependent gating mechanism which operates at very low internal $[Mg^{2+}]$. Raising $[Mg^{2+}]_i$ to 1.9 mM had only subtle effects on the IR conductance, broadening the activation curve by 20% and slightly increasing $I_{0,min}$. Whole-cell currents were studied with pipette solutions containing either 1.9 mM free Mg^{2+}, or no added Mg^{2+} and EDTA, ATP, or F^- as Mg^{2+} chelators or buffers. Experiments done with K-free pipette solutions, described in the Methods, indicate that there are no unusual barriers to diffusion of pipette constituents as large as NMG^+ to the cytoplasmic region at the inner end of IR channels. The equilibration times observed agree with those given by an empirical equation of Pusch and Neher (1988), consistent with the idea that our pipette solutions effectively replace the cytoplasm within the first few minutes of each experiment. Consideration of the possibility that external Mg^{2+} may cross the membrane and accumulate just under the membrane in a simple model described in Methods indicates that diffusion of Mg^{2+} into the pipette will reduce submembrane $[Mg^{2+}]$ to a few micromolar even without including the effects of Mg^{2+} buffers. The critical assumption in this calculation is that the Mg^{2+} permeability of barnacle muscle cells (Montes et al., 1989) is comparable to that in endothelial cells. If endothelial cells have a special Mg-transport mechanism then greater accumulation of Mg inside the membrane might occur. It would be useful to find a Mg-sensitive membrane protein that could be used as a bioassay for the local $[Mg^{2+}]$. For example, Na,K-ATPase activity is abolished in squid giant axons when $[Mg^{2+}]_i$ is reduced from 10 to 0 mM (Rakowski et al., 1989). Assuming a similar pump density, however, would predict only ~10 pA of pump current in the relatively small endothelial cells, and the sensitivity of the pump to $[Mg^{2+}]_i$ in the low micromolar range is unknown.

We were unable to detect any changes in IR gating as a function of time after achieving whole-cell configuration. Specifically, the slope factor of the activation curve did not detectably change with time. This parameter may have changed before the first measurement could be completed; however, removal of internal Mg^{2+} decreased k_n on average by only ~20%, a change which might not have been detected in any given experiment. Josephson (1988) reported that the whole-cell *I-V* relationship of the IR in chick ventricular myocytes was progressively linearized after several minutes of dialysis by a Mg-free pipette solution. In endothelial cells, in contrast, we never observed a tendency toward linearization of the *I-V*, even during experiments lasting 2–3 h. In some cells, outward currents which appeared to be unrelated to the IR (i.e., leak currents or some other conductance) became smaller with time, enhancing the negative conductance region of the *I-V* relationship.

Steady-State Voltage Dependence of the IR

The voltage-dependence of the IR originally was quantified in starfish egg cells by fitting the chord conductance with a Boltzmann function with a midpoint 15 mV negative to E_K and a slope factor of 6.7 mV (Hagiwara and Takahashi, 1974). Use of chord conductance does not discriminate between rectification due to resolvable gating and single-channel rectification, which might result from: (a) asymmetric K^+ concentrations, (b) intrinsic rectification due to the energy profile seen by a K^+ ion permeating a channel, or (c) an additional gating or blocking mechanism too fast to be resolved. In endothelial cells, the chord conductance-voltage relation is less steep than the activation curve estimated as in Fig. 4, with slope factors typically 20–40% larger (data not shown). In addition, conductance-voltage data decline less steeply with depolarization positive to E_K than does a Boltzmann fitted to the data at more negative potentials. These results indicate that the gating mechanism does not fully account for steady-state inward rectification. Similarly, when the voltage dependence of the IR of skeletal muscle is estimated by chord conductance measurements, slope factors of 11–12 mV are obtained (Hestrin, 1981; DeCoursey et al., 1984), while the activation curve determined by a procedure like that in Fig. 4 is steeper, with a slope factor of 7.5 mV (Leech and Stanfield, 1981). The activation curve in guinea pig heart has a slope factor of 7.2–8.0 mV (Tourneur et al., 1987; Saigusa and Matsuda, 1988); in canine Purkinje myocytes the slope factor was 5.6 mV with normal $[K^+]_i$ and less steep, 6.7 mV, with 25 mM $[K^+]_i$ (Cohen et al., 1989). The open probability vs. voltage relationship determined from single-channel measurements appears roughly comparable to activation curves from macroscopic measurements, with a slope factor of 5.4 mV for guinea pig ventricular myocytes (calculated from Kurachi, 1985) and 4.13 mV for mammalian skeletal muscle (Burton and Hutter, 1989). The latter measurements were made on inside-out patches exposed to Mg-free solutions, and therefore reflect intrinsic gating and not Mg^{2+} block. The slope factor found for endothelial cell IR gating with Mg-free solutions was 4.3 mV, which corresponds to about six gating charges moving across the whole membrane field.

The activation curve of IR in endothelial cells was slightly less steep in cells studied with 1.9 mM $[Mg^{2+}]_i$. Shown in Fig. 8 are steady-state currents calculated using mean values of V_n and k_n measured in Ringer's with and without internal Mg^{2+}. The increase in k_n by internal Mg^{2+} results in a small increase in the outward current and slightly extends the voltage range over which outward IR currents are present. This calculation assumes Goldman-Hodgkin-Katz rectification, but assuming a linear instantaneous *I-V* does not appreciably change the calculated currents. Compared with steady-state currents recorded in endothelial cells (Fig. 3), the calculated currents are generally similar even to the extent that high internal Mg^{2+} (Fig. 3 B) appears to extend the voltage range over which outward IR currents can be detected. Quantitatively however, the observed outward currents in Fig. 3 approach the voltage axis more gradually than the calculated currents. As discussed above, the chord conductance-voltage relation deviates from a Boltzmann fitted to more negative data points. Apparently, at potentials positive to E_K at which the macro-

scopic gating is at its minimum, there is still measurable outward current which decreases to a negligible amplitude more gradually than does the activation curve.

Limiting value of $I_{0,min}$. Since the demonstration of a time-dependent gating process of IR currents (Almers, 1971; Hagiwara et al., 1976), inward rectification observed during hyperpolarizing voltage pulses traditionally has been divided into instantaneous and time-dependent components. The instantaneous component in some studies is probably due in part to rectification of current through IR channels already open at the holding potential (e.g., Hestrin, 1981; DeCoursey et al., 1984). If all the IR channels are closed at positive potentials and if gating is first order, after large depolarizing prepulses the instantaneous component of inward rectification should vanish, as was observed for macroscopic IR currents in cat ventricular myocytes (Harvey and Ten Eick, 1988), and for ensemble averages of single-channel currents in guinea pig ventricle (Kurachi, 1985). However, in the present study as well as in earlier studies (Hagiwara et al., 1976; Leech and Stanfield, 1981; Tourneur
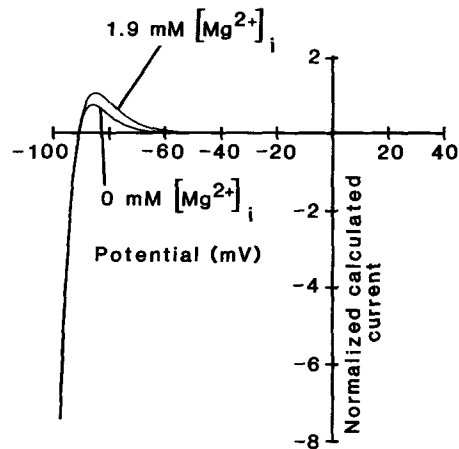

FIGURE 8. Steady-state IR currents calculated using the Goldman-Hodgkin-Katz current equation and mean values of V_n and k_n determined in 4.5 K^+ Ringer. The more gradual slope in cells with 1.9 $[Mg^{2+}]_i$ results in slightly larger outward current, visible over a wider voltage range. Currents were normalized as was done for real data in Fig. 3 by dividing currents by the slope conductance at -150 mV and plotted on similar axes.

et al., 1987), an instantaneous current jump upon hyperpolarization was sometimes seen even after large positive prepulses. In endothelial cells this limiting instantaneous conductance $(I_{0,min})$ averaged 0.31 of the total conductance when 1.9 mM $[Mg^{2+}]_i$ was present, similar to 0.27 in starfish egg (Hagiwara et al., 1976) and 0.43 in frog skeletal muscle (Leech and Stanfield, 1981). Both of the latter-mentioned studies were done on intact cells, presumably with substantial $[Mg^{2+}]_i$. When Mg-free pipette solutions were used in endothelial cells, $I_{0,min}$ was significantly smaller and was indistinguishable from zero in many experiments done in high $[K^+]_o$. This result suggests the possibility that at least part of the instantaneous component may be attributable to rapid unblock of IR channels which were open and blocked by internal Mg^{2+} at positive potentials. The instantaneous current measurement, however, depends critically upon both accurate leak subtraction and capacity compensation; the possibility that the apparent difference in $I_{0,min}$ may be due to a subtle effect of internal Mg^{2+} on the leak conductance cannot be excluded.

Kinetics of the Intrinsic Gating Mechanism of the IR

Studied in cells with divalent-free pipette solutions, the behavior of IR in endothelial cells can be approximated by a two-state gating mechanism. Both activation and deactivation rate constants are exponentially dependent on voltage, and the closing rate is twice as steeply voltage dependent, changing e-fold for 9 mV, compared with 18 mV for the opening rate. One consequence of these properties is that activation kinetics can be resolved over a wider voltage range than deactivation kinetics. Most studies of IR gating kinetics have been restricted to the kinetics of activation of inward current. When both activation and deactivation are studied, the IR time constant determined from macroscopic current measurements has a bell-shaped voltage dependence in starfish egg cells (Hagiwara et al., 1976), canine Purkinje myocytes (Cohen et al., 1989), guinea pig ventricular cells (Saigusa and Matusda, 1988), and frog skeletal muscle fibers (Almers, 1971; Hestrin, 1981), although Leech and Stanfield (1981) found that at least one component of deactivation in frog muscle became slower at more positive potentials. Similar to the present results, Saigusa and Matsuda (1988) found that deactivation was more steeply voltage dependent than activation; in addition they found that deactivation but not activation became more steeply voltage dependent when the internal potassium concentration, $[K^+]_i$, was increased.

The activation-deactivation process described here and in numerous macroscopic studies has been detected in only a few of the dozens of single-channel studies of IR channels in various preparations. Most single-channel studies involve channel inactivation at large negative potentials or channel block. The difficulty in resolving IR gating at the single-channel level is probably the result of (a) rapid gating kinetics, which become faster as the potential is changed away from the midpoint of the activation curve, (b) the steep voltage dependence of gating, which leaves only a narrow voltage range within which channels are likely to gate in the steady state, and (c) the dependence of gating on $[K^+]_o$ which with normal $[K^+]_i$ results in gating always occurring near E_K where the unitary currents are small. Potassium current noise attributed to IR channel gating was detected only 10–21 mV negative to E_K in skeletal muscle (DeCoursey et al., 1984). Kurachi (1985) observed rapid single-channel fluctuations attributed to activation gating in cardiac muscle, in addition to slower events at large negative potentials attributed to inactivation. The single-channel data that exist are generally consistent with the present result; gating was describable as a two-state process with a bell-shaped τ-voltage relationship and a steep steady-state activation curve (Kurachi, 1985; Burton and Hutter, 1989).

Instantaneous current-voltage relation. In the present study, the instantaneous current-voltage relation of the IR of endothelial cells could not be resolved reliably more than ~20 mV positive to E_K (Fig. 5). It is thus not possible to determine whether internal Mg^{2+} causes instantaneous rectification by rapid open-channel block as found in single-channel studies (Matsuda et al., 1987; Vandenberg, 1987; Burton and Hutter, 1989). However, the observation that both transient and maintained outward currents can be detected in endothelial cells with 1.9 mM $[Mg^{2+}]_i$ indicates that IR channels in endothelial cells must be relatively insensitive to internal Mg^{2+}. The IR channel of endothelial cells may have a sensitivity to $[Mg^{2+}]_i$

in the millimolar range, as has been reported for a variety of channels including ATP-sensitive K^+ channels (Horie et al., 1987) and muscarinic K^+ channels (Horie and Irisawa, 1989) in guinea pig myocytes, ATP-sensitive and Ca-dependent K^+ channels in an insulin-secreting cell line (Ribalet et al., 1988), and sodium channels in *Xenopus* oocytes (Pusch et al., 1989).

Physiological function of IR in endothelial cells. Since the resting membrane potential of endothelial cells, estimated as the zero-current potential in whole-cell recordings to be -56 to -77 mV (Colden-Stanfield, et al., 1987; Fichtner et al., 1987; Johns et al., 1987; Takeda et al., 1987; Olesen et al., 1988a), is more positive than E_K, IR channels in intact cells could carry only outward current under physiological conditions. No outward currents attributable to IR channels were detected in previous studies of endothelial cells (Johns et al., 1987; Takeda et al., 1987), although small outward IR currents have long been recognized in other cells (e.g., Adrian and Freygang, 1962; Hagiwara et al., 1976). Takeda et al. (1987) argued that the IR in endothelial cells is unlikely to contribute to setting the resting potential because of the absence of outward currents. We describe here both transient and maintained outward IR currents. Our results then, support the idea that the IR of endothelial cells helps maintain the resting potential, as suggested by the depolarizing effect of Ba^{2+} (Johns et al., 1987). Since endothelial cells apparently lack depolarization-activated fast inward current channels (Colden-Stanfield et al., 1987; Johns et al., 1987; Takeda et al., 1987) such as Na^+ or Ca^{2+} channels, they would not be expected to undergo action potentials or other rapid regenerative voltage changes; thus the time-independent component of outward IR current may be more important in intact endothelial cells than the transient component.

This study demonstrates that the voltage-, time-, and $[K^+]_o$-dependent current relaxations of the IR of endothelial cells are similar with high and low $[Mg^{2+}]_i$, and are therefore most simply explainable as the result of an intrinsic gating mechanism, and not voltage- and time-dependent block by internal Mg^{2+}. The gating mechanism of the IR of endothelial cells thus may be the result of voltage-dependent conformational changes of the channel protein, like that of other voltage-dependent channels. The dependence of IR gating on $[K^+]_o$ (Hagiwara and Yoshii, 1979), and to a lesser extent also on $[K^+]_i$ (Hestrin, 1981; Saigusa and Matsuda, 1988; Cohen et al., 1989), remains a unique feature which must be considered in any model of gating (e.g., Ciani et al., 1978; Ciani, 1982). Hille and Schwarz (1978) could account for most properties of inward rectification by a blocking ion mechanism. To reproduce the steep voltage dependence of the IR observed in endothelial cells, with an effective valence of six charges, would require a large number of binding sites in the channel for a monovalent blocker. Increasing the valence of the blocking ion to two in the Hille-Schwarz model steepened the voltage dependence of block, but then the block no longer shifted in parallel with changes in E_K when $[K^+]_o$ was changed. Table II shows that the activation curve of the endothelial cell IR shifts strictly along with V_K, which in the Hille and Schwarz model is therefore more consistent with a monovalent gating particle. In conclusion, compared with its role in cardiac myocytes, internal Mg^{2+} appears to play a relatively minor role in the mechanism of inward rectification in endothelial cells.

REFERENCES

Adrian, R. H., and W. H. Freygang. 1962. Potassium conductance of frog muscle membrane under controlled voltage. *Journal of Physiology.* 163:104–114.

Almers, W. 1971. The potassium permeability of frog muscle membrane. Ph.D. Thesis. University of Rochester, Rochester, NY.

Armstrong, C. M. 1975. Potassium pores of nerve and muscle membranes. *In* Membranes-a Series of Advances. Chapter 5. G. Eisenman, editor. Marcel Dekker, New York. 325–358.

Armstrong, C. M., and L. Binstock. 1965. Anomalous rectification in the squid giant axon injected with tetraethylammonium chloride. *Journal of General Physiology.* 48:859–872.

Bakhramov, A., P. Bregestovski, and K. Takeda. 1988. Histamine-dependent currents in endothelial cells isolated from human umbilical vein. *Journal of Physiology.* 406:90P. (Abstr.)

Biermans, G., J. Vereecke, and E. Carmeliet. 1987. The mechanism of the inactivation of the inward-rectifying K current during hyperpolarizing steps in guinea-pig ventricular myocytes. *Pflügers Archiv.* 410:604–613.

Blatter, L. A., and J. A. S. McGuigan. 1986. Free intracellular magnesium concentration in ferret ventricular muscle measured with ion selective micro-electrodes. *Quarterly Journal of Experimental Physiology.* 71:467–473.

Burton, F. L., and O. F. Hutter, 1989. Properties of 'inwardly rectifying' potassium channels from mammalian sarcolemmal vesicles in absence of "intracellular" Mg^{2+}. *Journal of Physiology.* 409:51P. (Abstr.)

Ciani, S. 1982. Theoretical study of the relaxation currents in voltage-clamp conditions as deduced from two models for "inward" rectification: the "blocking particle" and the "electrochemical gating" hypotheses. *Journal of Theoretical Neurobiology.* 1:228–248.

Ciani, S., S. Krasne, S. Miyazaki, and S. Hagiwara. 1978. A model of anomalous rectification: electrochemical-potential-dependent gating of membrane channels. *Journal of Membrane Biology.* 44:103–134.

Cohen, I. S., D. DiFrancesco, N. K. Mulrine, and P. Pennefather. 1989. Internal and external K^+ help gate the inward rectifier. *Biophysical Journal.* 55:197–202.

Colden-Stanfield, M., W. P. Schilling, A. K. Ritchie, S. G. Eskin, L. T. Navarro, and D. L. Kunze. 1987. Bradykinin-induced increases in cytosolic calcium and ionic currents in cultured bovine aortic endothelial cells. *Circulation Research.* 61:632–640.

Conner, J. A., and C. F. Stevens. 1971. Voltage clamp studies of a transient outward current in gastropod neural somata. *Journal of Physiology.* 213:21–30.

Cota, G., and C. M. Armstrong. 1988. Potassium channel "inactivation" induced by soft-glass pipettes. *Biophysical Journal.* 53:107–109.

DeCoursey, T. E., J. Dempster, and O. F. Hutter. 1984. Inward rectifier current noise in frog skeletal muscle. *Journal of Physiology.* 349:299–327.

Fanburg, B. L. 1988. Relationship of the pulmonary vascular endothelium to altered pulmonary vascular resistance: state of the art. *Chest.* 93:101S–105S.

Fichtner, H., U. Fröbe, R. Busse, and M. Kohlhardt. 1987. Single nonselective cation channels and Ca^{2+}-activated K^+ channels in aortic endothelial cells. *Journal of Membrane Biology.* 98:125–133.

Furman, R. E., and J. C. Tanaka. 1988. Patch electrode glass composition affects ion channel currents. *Biophysical Journal.* 53:287–292.

Godt, R. E., and D. W. Maughan. 1988. On the composition of the cytosol of relaxed skeletal muscle of the frog. *American Journal of Physiology.* 254:C591–C604.

Hagiwara, S., S. Miyazaki, W. Moody, and J. Patlak. 1978. Blocking effects of barium and hydrogen ions on the potassium current during anomalous rectification in the starfish egg. *Journal of Physiology.* 279:167–185.

Hagiwara, S., S. Miyazaki, and N. P. Rosenthal. 1976. Potassium current and the effect of cesium on this current during anomalous rectification of the egg cell membrane of a starfish. *Journal of General Physiology.* 67:621–638.

Hagiwara, S., and K. Takahashi. 1974. The anomalous rectification and cation selectivity of the membrane of a starfish egg cell. *Journal of Membrane Biology.* 18:61–80.

Hagiwara, S., and M. Yoshii. 1979. Effects of internal potassium and sodium on the anomalous rectification of the starfish egg as examined by internal perfusion. *Journal of Physiology.* 292:251–265.

Harvey, R. D., and R. E. Ten Eick. 1988. Characterization of the inward-rectifying potassium current in cat ventricular myocytes. *Journal of General Physiology.* 91:593–615.

Henderson, P. 1907. Zur thermodynamik der Flüssigkeitsketten. *Zeitschrift der Physische Chemie.* 59:118–127.

Hestrin, S. 1981. The interaction of potassium with the activation of anomalous rectification in frog muscle membrane. *Journal of Physiology.* 317:497–508.

Hille, B. 1977. The pH-dependent rate of action of local anesthetics on the node of Ranvier. *Journal of General Physiology.* 69:475–496.

Hille, B., and W. Schwarz. 1978. Potassium channels as multi-ion single-file pores. *Journal of General Physiology.* 72:409–442.

Horie, M., and H. Irisawa, 1989. Dual effects of intracellular magnesium on muscarinic potassium channel current in single guinea-pig atrial cells. *Journal of Physiology.* 408:313–332.

Horie, M., H. Irisawa, and A. Noma. 1987. Voltage-dependent magnesium block of adenosine-triphosphate-sensitive potassium channel in guinea-pig ventricular cells. *Journal of Physiology.* 387:251–272.

Jaffe, E. A., I. W. Hoyer, and R. L. Nachman. 1973. Synthesis of antihemophilic factor antigen by cultured human endothelial cells. *Journal of Clinical Investigation.* 52:2757–2764.

Johns, A., T. W. Lategan, N. J. Lodge, U. S. Ryan, C. van Breeman, and D. Adams. 1987. Calcium entry through receptor-operated channels in bovine pulmonary artery endothelial cells. *Tissue and Cell.* 19:733–745.

Josephson, I. R. 1988. Properties of inwardly rectifying K^+ channels in ventricular myocytes. *Molecular and Cellular Biochemistry.* 80:21–26.

Kurachi, Y. 1985. Voltage dependent activation of the inward rectifier potassium channel in the ventricular cell membrane of the guinea-pig heart. *Journal of Physiology.* 336:365–385.

Landolt-Börnstein. 1960. Zahlenwerte and Funktionen. II. Band. Eigenschaften der Materie in Ihren Aggregatzuständen. 7. Teil. Elektrische Eigenschaften II. K. H. Hellwege, A. M. Hellwege, K. Schäfer, and E. Lax, editors. Springer-Verlag, Berlin. 264-266.

Lansman, J. B., T. J. Hallam, and T. J. Rink. 1987. Single stretch-activated ion channels in vascular endothelial cells as mechanotransducers? *Nature.* 325:811–813.

Leech, C. A., and P. R. Stanfield. 1981. Inward rectification in frog skeletal muscle fibres and its dependence on membrane potential and external potassium. *Journal of Physiology.* 319:295–309.

Martell, A. E., and R. M. Smith. 1974. Critical Stability Constants. Vol. 1, Amino Acids. Plenum Publishing Co., New York.

Marty, A., and E. Neher. 1983. Tight-seal whole-cell recording. *In* Single Channel Recording. Chapter 7. B. Sakmann and E. Neher, editors. Plenum Publishing Co., New York. 107–122.

Mathias, R. T., I. Cohen, and C. Oliva. 1989. Some limitations of the whole cell patch clamp technique in the study of membrane transport. *Biophysical Journal.* 55:44a. (Abstr.)

Matsuda, H. 1988. Open-state substructure of inwardly rectifying potassium channels revealed by magnesium block in guinea-pig heart cells. *Journal of Physiology.* 397:237–258.

Matsuda, H., A. Saigusa, and H. Irisawa. 1987. Ohmic conductance through the inwardly rectifying K channel and blocking by internal Mg^{2+}. *Nature.* 325:156–159.

Mitra, R., and M. Morad. 1987. Block by Ba^{2+}, Sr^{2+}, Ca^{2+} of Cs^+, Rb^+, and K^+ currents through inwardly rectifying K^+ channel in isolated guinea pig ventricular myocytes: implications on channel gating. *Biophysical Journal.* 51:367a. (Abstr.)

Montes, J. G., R. A. Sjodin, A. L. Yergey, and N. E. Vieira. 1989. Simultaneous bidirectional magnesium ion flux measurements in single barnacle muscle cells by mass spectrometry. *Biophysical Journal.* 56:437–446.

Murphy, E., C. C. Freudenrich, L. A. Levy, R. E. London, and M. Lieberman. 1989. Monitoring cytosolic free magnesium in cultured chicken heart cells by use of the fluorescent indicator Furaptra. *Proceedings of the National Academy of Sciences.* 86:2981–2984.

Neher, E. 1971. Two transient current components during voltage clamp in snail neurons. *Journal of General Physiology.* 61:385–399.

Ohmori, H. 1978. Inactivation kinetics and steady-state current noise in the anomalous rectifier of tunicate egg cell membranes. *Journal of Physiology.* 281:77–99.

Olesen, S. P., D. E. Clapham, and P. F. Davies. 1988a. Haemodynamic shear stress activates a K^+ current in vascular endothelial cells. *Nature.* 331:168–170.

Olesen, S. P., P. F. Davies, and D. E. Clapham. 1988b. Muscarinic-activated K^+ current in bovine aortic endothelial cells. *Circulation Research.* 62:1059–1064.

Pusch, M., F. Conti, and W. Stühmer. 1989. Block of Na^+ outward currents by intracellular Mg^{2+}. *Biophysical Journal.* 55:311a. (Abstr.)

Pusch, M., and E. Neher. 1988. Rates of diffusional exchange between small cells and a measuring patch pipette. *Pflügers Archiv.* 411:204–211.

Rae, J. L., and R. A. Levis. 1984. Patch voltage clamp of lens epithelial cells: theory and practice. *Molecular Physiology.* 6:115–162.

Raju, B., E. Murphy, L. A. Levy, R. D. Hall, and R. E. London. 1989. A fluorescent indicator for measuring cytosolic free magnesium. *American Journal of Physiology.* 25:C540–548.

Rakowski, R. F., D. C. Gadsby, and P. DeWeer. 1989. Stoichiometry and voltage dependence of the sodium pump in voltage-clamped, internally dialyzed squid giant axon. *Journal of General Physiology.* 93:903–941.

Ribalet, B., S. Ciani, and G. T. Eddelstone. 1988. Magnesium blockage of two K channels in an insulin-secreting cell line. *Biophysical Journal.* 53:549a. (Abstr.)

Robinson, R. A., and R. H. Stokes. 1965. Electrolyte Solutions. Butterworths, London.

Rubin, D. B., E. A. Drab, W. F. Ward, L. J. Smith, and S. M. Fowell. 1984. Enzymatic responses to radiation in cultured vascular endothelial and smooth muscle cells. *Radiation Research.* 99:420–432.

Ryan, J. W., A. Chung, L. D. Martin, and U. S. Ryan. 1978a. New substrates for the radioassay of angiotensin converting enzyme of endothelial cells in culture. *Tissue and Cell.* 10:555–562.

Ryan, U. S., E. Clements, D. Habliston, and J. W. Ryan. 1978b. Isolation and culture of pulmonary artery endothelial cells. *Tissue and Cell.* 10:535–554.

Saigusa, A., and H. Matsuda. 1988. Outward currents through the inwardly rectifying potassium channel of guinea-pig ventricular cells. *Japanese Journal of Physiology.* 38:77–91.

Sauve, R., L. Parent, C. Simoneau, and G. Roy. 1988. External ATP triggers a biphasic activation process of a calcium-dependent K^+ channel in cultured bovine aortic endothelial cells. *Pflügers Archiv.* 412:469–481.

Silver, M. R., and T. E. DeCoursey. 1989. Inward rectifier channels in endothelial cells are not gated by internal magnesium. *Biophysical Journal.* 55:6a. (Abstr.)

Silver, M. R., E. R. Jacobs, and T. E. DeCoursey. 1987. Inward rectifier channels in bovine pulmonary artery endothelial cells. *American Review of Respiratory Disease.* 133:A89. (Abstr.)

Standen, N. B., and P. R. Stanfield. 1978a. Inward rectification in skeletal muscle: a blocking particle model. *Pflügers Archiv.* 378:173–176.

Standen, N. B., and P. R. Stanfield. 1978b. A potential- and time-dependent blockade of inward rectification in frog skeletal muscle fibres by barium ions and strontium ions. *Journal of Physiology.* 280:169–191.

Standen, N. B., and P. R. Stanfield. 1979. Potassium depletion and sodium block of potassium currents under hyperpolarization in frog sartorius muscle. *Journal of Physiology.* 294:497–520.

Takeda, K., V. Schini, and H. Stoekel. 1987. Voltage-activated potassium, but not calcium currents in cultured bovine aortic endothelial cells. *Pflügers Archiv.* 410:385–393.

Tessier-Lavigne, M., D. Attwell, P. Mobbs, and M. Wilson. 1988. Membrane currents in retinal bipolar cells of the axolotl. *Journal of General Physiology.* 91:49–72.

Tourneur, Y., R. Mitra, M. Morad, and O. Rougier. 1987. Activation properties of the inward-rectifying potassium channel on mammalian heart cells. *Journal of Membrane Biology.* 97:127–135.

Vandenberg, C. A. 1987. Inward rectification of a potassium channel in cardiac ventricular cells depends on internal magnesium ions. *Proceedings of the National Academy of Sciences.* 84:2560–2564.

Vanhoutte, P. M. 1987. The end of the quest? *Nature.* 327:459–460.

Weast, R. C. 1987. CRC Handbook of Chemistry and Physics. R. C. Weast, editor. CRC Press, Inc., Boca Raton, FL.